# Constrained optimal control:
# an application to semiactive suspension systems

Tina Paschedag, Alessandro Giua, Carla Seatzu

*Abstract*— **This paper compares three different control design methods with regard to their application to a quarter car semiactive suspension model, namely *optimal gain switching*, *discontinuous variable structure control* and *explicit model predictive control*. All of them divide the state space into convex regions and assign one linear or affine state feedback controller to each region. The partition of the state space is computed off-line. During the on-line phase, the controller switches between the subcontrollers according to the current state.**

## I. INTRODUCTION

In this paper we consider *linear systems with constraints*. It is well accepted that for these systems, in general, stability and good performance can only be achieved with a non-linear control law. Here we investigated three different approaches to design a non-linear controller for linear constrained systems, namely *optimal gain switching* (OGS) [16], *discontinuous variable structure control* (dVSC) [1], [2], [10] and *explicit model predictive control* (eMPC) [3], [5]. All these methods consist of an off-line and an on-line phase. The off-line phase divide the state space into several regions and assign them linear subcontrollers in the case of OGS and dVSC, and affine subcontrollers in the case of eMPC. During the on-line phase the controller switches between these subcontrollers according to the current system state.

A first remark is in order: of the three approaches eMPC is the most general in the sense that it can take into account general constraints of the form

$$V_u u(t) + V_x x(t) \leq V \tag{1}$$

where $u(t) \in \mathbb{R}^r$ is the control input, $x(t) \in \mathbb{R}^n$ is the state and $V_u$, $V_x$ and $V$ are matrices of suitable dimension. On the contrary, the other two approaches can only deal with *symmetric* constraints of the form

$$|u(t) - k^T x(t)| \leq u_{max} \tag{2}$$

where $u(t) \in \mathbb{R}$ is a scalar input and $k \in \mathbb{R}^n$ is a constant gain vector. Constraints (2) are obviously a particular case of (1).

To compare the three design methods, we applied them to a quarter-car suspension system, where the constraint on the input takes the form $|u(t)| \leq u_{\max}$, i.e., is a special case of (2). The three approaches can be used for the design of *active* control laws, that we then approximate using a *semiactive* suspension system.

T. Paschedag is with the Istitute of Automation Technology, Otto-von Guericke University Magdeburg, {Tina.Paschedag@web.de.

A. Giua and C. Seatzu are with the Department of Electrical and Electronic Engineering, University of Cagliari, {giua,seatzu}@diee.unica.it.

The design of active suspensions for road vehicles aims to optimize the performance of the vehicle with regard to comfort, road holding and rideability [9], [14]. In an active suspension the interaction between vehicle body, the so-called sprung mass, and wheel (nonsprung mass) is regulated by an actuator of variable length. The actuator is usually hydraulically controlled and applies between body and wheel a force that represents the control action generally determined with an optimization procedure [8].

In contrast to active suspensions, passive suspensions consist of dampers and springs and the interaction between body and wheel is determined by their elastic constants and damping coefficients, that are constant.

Active suspensions have a better performance than passive suspensions, but they are much more complex and expensive. As a viable alternative to a purely active suspension system, the use of semiactive suspensions has been investigated a lot in the past [6], [11]. Such a system consists of a spring whose stiffness is constant and of a damper whose characteristic coefficient $f$ is adjustable within an interval $[f_{\min}, f_{\max}]$. The value $f$ is determined such that an active control considered as target is approximated as close as possible.

The control design and simulation results are presented in a series of figures that, given the page limitation, are small. A file containing all figures in larger scale can be found at http:\\kalman.diee.unica.it\giua\MED06\figs.pdf.

## II. DYNAMICAL MODEL OF THE SUSPENSION SYSTEM

In this paper we consider two different dynamical models of a quarter-car suspension system. The first one is a two-degrees of freedom fourth-order model [8]. The second one is a one-degree of freedom second-order model that neglects the dynamics of the tire.

Since the reduced model does not describe the interaction of the tire with the suspended mass and the ground, it cannot be used to evaluate features like road holding and rideability. However, as it will be discussed later, it allows a significant comparison among the different design techniques we considered.

### A. The Two-Degrees of Freedom Model

The two-degrees of freedom model is depicted in Fig. 1.a (active suspension) and b (semiactive suspension), where we used the following notation: $M_w$ is the nonsprung mass consisting of the wheel and its moving parts; $M_s$ is the sprung mass, i.e. the part of the whole body mass and the load mass pertaining to only one wheel; $x_1(t)$ is the nonsprung mass displacement at time $t$ with respect to a
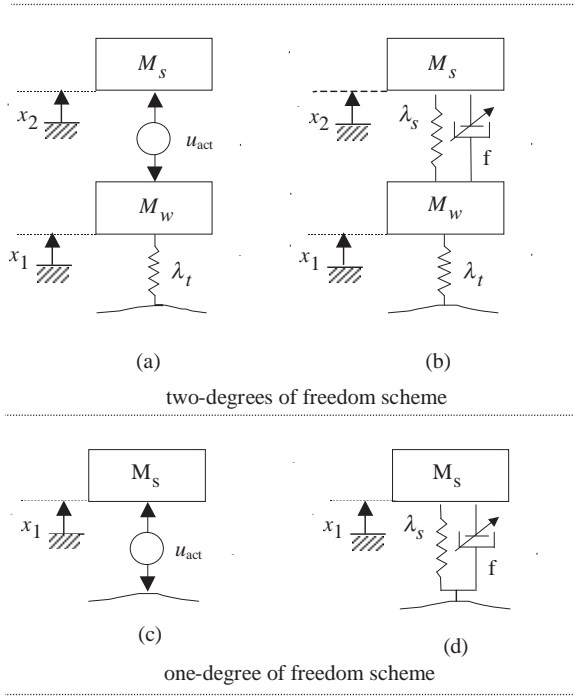
Fig. 1. Model of the two-degrees of freedom model (a) active (b) semiactive suspension; model of the one-degree of freedom model (c) active (d) semiactive suspension;

fixed reference; $x_2(t)$ is the sprung mass displacement at time $t$ with respect to a fixed reference; $x_3(t) = \dot{x}_1(t)$ is the velocity of the nonsprung mass at time $t$; $x_4(t) = \dot{x}_2(t)$ is the velocity of the sprung mass at time $t$; $u_{\text{act}}(t)$ is the active control force at time $t$; $\lambda_t$ is the elastic constant of the tire, whose damping characteristics have been neglected. This is in line with almost all researchers who have investigated synthesis of active suspensions for motor vehicles as the tire damping is minimal; $\lambda_s$ is the elastic constant of the spring of the semiactive suspension; $f(t)$ is the adjustable damper coefficient of the semiactive suspension at time $t$.

The state space model of the active suspension is governed by the following state equation

$$\dot{x}(t) = A x(t) + B u(t) \tag{3}$$

where

$$A = \begin{bmatrix} 0 & 0 & 1 & 0 \\ 0 & 0 & 0 & 1 \\ -\frac{\lambda_t}{M_w} & 0 & 0 & 0 \\ 0 & 0 & 0 & 0 \end{bmatrix}, \quad B = \begin{bmatrix} 0 \\ 0 \\ -\frac{1}{M_w} \\ \frac{1}{M_s} \end{bmatrix}.$$

The control force should satisfy the following constraint:

$$|u_{\text{act}}(t)| \leq u_{\text{max}}. \tag{4}$$

This constraint bounds the acceleration of the sprung mass – at least in nominal operating conditions, i.e., when the linear model of the suspension is valid – so as to ensure the confort of the passengers. Furthermore, this constraint limits the maximal force required from the controller, i.e., it leads to the choice of a suitable actuator.

The control laws we propose all requires the knowledge of the system's state $x$[1].

Since both the concepts of OGS and eMPT make use of a discrete-time state space model, we choose a sampling interval $T$ and discretize[2] the model (3), thus getting the new model

$$x(k+1) = G x(k) + H u(k) \tag{5}$$

where

$$G = e^{AT}, \qquad H = \left( \int_0^T e^{A\tau} d\tau \right) B. \tag{6}$$

The effect of the semiactive suspension which is composed of a spring and a damper with an adjustable damper coefficient (see Fig. 1.b) leads to the semiactive control law $u_{\text{sem}}(k) = -[-\lambda_s \quad \lambda_s \quad -f(k) \quad f(k)] \cdot x(k)$.

Note that, as $f$ may vary, $u_{\text{sem}}(k)$ is both a function of $f$ and of $x(k)$.

In general, $f$ may only take values in a real set $[f_{\text{min}}, f_{\text{max}}]$. We propose to choose at each step $k$ the value of $f(k)$ to minimize the difference $F[f, x(k)] = (u_{\text{act}}(k) - u_{\text{sem}}(k))^2$. Let us first assume $x_3(k) \neq x_4(k)$, then the value $f^*(k)$ such that $F[f^*(k), x(k)] = 0$ is

$$f^*(k) = -\frac{u_{\text{act}}(k) + \lambda_s \, \Delta x(k)}{\Delta v(k)} \tag{7}$$

where $\Delta x(k) = x_2(k) - x_1(k)$ is the suspension deformation and $\Delta v(k) = x_4(k) - x_3(k)$ is its rate of change.

As the admissible values of $f$ lie in the interval $[f_{\text{min}}, f_{\text{max}}]$ the adjusted damper coefficient becomes

$$f(k) = \text{minarg}_{f \in [f_{\text{min}}, f_{\text{max}}]} F[f, x(k)] = \begin{cases} f_{\text{max}} & \text{if} \quad f^*(k) > f_{\text{max}} \\ f^*(k) & \text{if} \quad f^*(k) \in [f_{\text{min}}, f_{\text{max}}] \\ f_{\text{min}} & \text{if} \quad f^*(k) < f_{\text{min}} \end{cases} \tag{8}$$

When $x_3(k) = x_4(k)$, regardless to the values of $f$, the damper does not give any contribution to $u_{\text{sem}}(k)$. Thus, in this case we assume $f(k) = f_{\text{max}}$, which we choose also as the initial value for the damper coefficient $f(0) = f_{\text{max}}$.

*B. The One-Degree of Freedom Model*

The one-degree of freedom model of the suspension system is schematized in Fig. 1.c (active suspension) and d (semiactive suspension), where we used the following new

---

[1]Since not every component of $x(t)$ is directly measurable, we reconstruct the state through an appropriate state observer. To do this, we choose a suitable output $y(t) = Cx(t)$, with $C = [1 \; -1 \; 0 \; 0; \; 0 \; 0 \; 0 \; 1]$, which corresponds to measuring the suspension deformation and the sprung mass velocity. The resulting system is thus observable and controllable.

[2]It is well known [13] that a system that is observable and controllable in the absence of sampling maintains these properties after the introduction of sampling if and only if, for every eigenvalue of $A$ for the continuous time control system, the relationship $Re\{\lambda_i\} = Re\{\lambda_j\}$ implies $Im\{\lambda_i - \lambda_j\} \neq \frac{2n\pi}{T}$, $n = \pm 1, \pm 2, \ldots$. The problem at hand results in the following set of eigenvalues: $\left\{0, 0, \sqrt{-\frac{\lambda_t}{M_w}}, -\sqrt{-\frac{\lambda_t}{M_w}}\right\}$. Under these conditions it is necessary to choose a sampling period $T$, such that: $T \neq n\pi \sqrt{\frac{M_w}{\lambda_t}}$.

notation: $x_1(t)$ is the sprung mass displacement at time $t$ with respect to a fixed reference; $x_2(t) = \dot{x}_1(t)$ is the velocity of the sprung mass at time $t$. The continuous-time state space model is in the form (3) with constraint (4), and

$$A = \begin{bmatrix} 0 & 1 \\ 0 & 0 \end{bmatrix}, \quad B = \begin{bmatrix} 0 \\ 1/M_s \end{bmatrix}.$$

while the discrete-time model can be obtained using eq. (6). Finally, the effect of the semiactive suspension is equivalent to that of a control force $u_{\text{sem}}(k) = -[\lambda_s \quad f(k)]\, x(k)$. Thus, minimizing $(u_{\text{act}}(k) - u_{\text{sem}}(k))^2$ under the assumption $x_2(k) \neq 0$, results in a damper coefficient

$$f^*(k) = -\frac{u_{\text{act}} - \lambda_s\, x_1(k)}{x_2(k)}. \tag{9}$$

As the damper coefficient has to be chosen out of the set $[f_{\min}, f_{\max}]$, $f(k)$ is determined considering (8).

### III. OPTIMAL GAIN SWITCHING

Let us consider a linear and time-invariant system

$$x(k+1) = Gx(k) + Hu(k). \tag{10}$$

We want to determine the control law $u^*(\cdot)$ that minimizes a performance index of the form:

$$J = \sum_{k=0}^{\infty} x^T(k)Q\, x(k), \tag{11}$$

(with $Q$ positive semidefinite) under the constraint

$$|u(k)| \leq u_{max} \quad (k \geq 0). \tag{12}$$

It is well known that the optimal solution $u^*(\cdot)$ does not correspond to a feedback control law, thus its application may be unfeasible [15].

The OGS approach, firstly proposed by Yoshida in [16] approximates the optimal control law $u^*(\cdot)$ by switching among a certain number of feedback control laws whose gains can be computed as the solution of a family of LQR problems. More precisely, to determine the OGS control law $u_{\text{OGS}}$ we consider a family of performance indices

$$J_\rho = \sum_{k=0}^{\infty} [\rho\, x^T(k)Q\, x(k) + u^T(k)Ru(k)], \quad \rho > 0,\ R > 0. \tag{13}$$

For a given value of $\rho$, the unconstrained control law that minimizes $J_\rho$ can be written as

$$u_\rho(k) = -K_\rho\, x(k) \tag{14}$$

where the gain matrix $K_\rho$ is obtained by solving an algebraic Riccati equation. The resulting controller then switches among different control laws in the form (14) depending on the current value of the system state.

For a given value of $\rho$ it is possible to compute a *linear region* $\Gamma_\rho$ in the state space such that for any point $x_0$ within this region the following equation holds:

$$|u_\rho(k)| \equiv |K_\rho(G - HK_\rho)^k\, x_0| \leq u_{max}, \quad (k \geq 0). \tag{15}$$

Thus, considering the system (10) controlled with $u_\rho$ and an initial state $x_0 \in \Gamma_\rho$, we can be sure that in its future evolution the value of the control input will always satisfy the constraint (12).

A finite set of $m$ values of $\rho$, namely $\{\rho_1, \ldots, \rho_m\}$ should be first selected[3]. Then, following a simple procedure given in [16], the regions $\Gamma_\rho$'s are computed off-line. Such a procedure, that is not reported here for brevity's requirements, is based on the solution of $m$ linear programming problems that provide appropriate matrices $Z_\rho$'s. At each sampling time $k$ the on-line phase of the approach simply requires to determine the largest value $v$ such that

$$v = \max\{\, i \mid x(k) \in \Gamma_{\rho_i},\ i = 0, \ldots, m\} \tag{17}$$

and set $\rho(k) = \rho_v$. The condition $x(k) \in \Gamma_\rho$ is true iff

$$-u_{\max} \leq Z_\rho x_0 \leq u_{\max}. \tag{18}$$

Thus the control law at time $k$ is chosen equal to

$$u_{\text{OGS}}(k) = -K_{\rho_v}. \tag{19}$$

It has been shown by Yoshida that if no disturbance is acting on the system, $\rho(k)$ is a nondecreasing function of $k$.

### IV. DISCONTINUOUS VARIABLE STRUCTURE CONTROL

The basic ideas of discontinuous VSC (dVSC) have been firstly proposed by Kiendl and Schneider [10], and a suitable design method was presented by Adamy [1]. Most of the literature on this topic is in German, but a good survey in English is available [2].

Similar to the OGS method the variable structure controller, depending on the system's state, either switches between a finite number of linear subcontrollers (discontinuous VSC) or changes the controller parameters continuously (soft VSC) with the objective of obtaining a better performance in terms of shorter settling times avoiding violation of control signal constraints.

The dVSC method makes use of a set of nested, positively invariant sets each with a dedicated linear controller. During the regulation cycle, the trajectory runs from a positively invariant region in the state space into the next smaller one simultaneously activating the assigned controller.

Here we briefly outline the general structure of the dVSC. Consider the linear time-invariant plant in continuous time

$$\dot{x}(t) = Ax(t) + Bu(t) \tag{20}$$

---

[3]The selection of the weighting coefficients needs some further comments. A good choice of the values $\rho_i$ may influence the performance of the OGS law. As $m$ increases, the performance index $J_\rho$ decreases, but the procedure becomes computationally more intensive. The weighting coefficient $\rho_1$ should be determined such that the linear region $\Gamma_{\rho_1}$ contains all the initial conditions of interest. The weighting coefficient $\rho_m$ should be selected such that the region $\Gamma_{\rho_m}$ covers small disturbances or very small system noises. The coefficients $\rho_2, \ldots, \rho_{m-1}$ should be chosen taking into account the size of the linear region $\Gamma_i$. Once $\rho_1$, $\rho_m$ and $m$ are determined, the intermediate values of $\rho$ can be chosen such that the ratios of the norm between two adjacent gains are constant, i.e.,

$$\frac{\|K_{\rho_i}\|}{\|K_{\rho_{i-1}}\|} = \left(\frac{\|K_{\rho_m}\|}{\|K_{\rho_1}\|}\right)^{\frac{1}{m}}. \tag{16}$$

under the control signal constraint

$$|u(t)| \leq u_{\max}. \tag{21}$$

The control input is chosen according to

$$u_{dVSC}(t) = \mathcal{F}(x(t), p) \tag{22}$$

where $\mathcal{F}$ is an operator[4] that depends on the system's state $x$ and a selection parameter $p$, that is computed by a selection strategy or supervisor, i.e., $p = S(x)$, defined by a discontinuous function $S$. The selection strategy switches between a finite number $m$ of different subcontrollers so as to optimize the system's performance in terms of *settling times*.

Note that in the following we consider only bounded sets $X_0 \subset \mathbb{R}^n$ of possible initial vectors $x(t = 0)$, since $X_0 = \mathbb{R}^n$ is usually not of practical interest. The three major steps of the dVSC design procedure are:

(D1) Choose a family of $m$ linear state controllers $u(t) = -K_p x(t)$ leading to stable control loops

$$\dot{x}(t) = (A - BK_p)\, x(t) = \hat{A}_p\, x(t), \quad p = 1, \ldots, m \tag{23}$$

whose response times decrease with increasing index $p$.

(D2) According to each control loop (23) construct a Lyapunov region

$$G_p = \{x \mid v_p(x) < c_p\} \tag{24}$$

where $c_p$ determines the size of $G_p$. Moreover, $G_p$ should be such that all $x \in G_p$ satisfy the constraint $|u_{dVSC}| = |K_p x| \leq u_{\max}$.

(D3) The Lyapunov regions should be nested one inside the other in accordance with

$$G_{p+1} \subset G_p, \quad p = 1, \ldots, k - 1 \tag{25}$$

with an increasing index $p$.

Analogously to the OGS design process the dVSC method consists of an off-line and an on-line phase. The three steps mentioned above represent the off-line phase. During the on-line phase the controller determines the smallest Lyapunov region that contains the current system's state and activates the subcontroller belonging to this region. Upon the trajectory's entry into a smaller region, the controller switches to the next assigned subcontroller.

In the first step the subcontrollers' matrices $K_p$ are determined utilizing *pole placement* such that the $n$ eigenvalues $\lambda_{p,j}$ of $\hat{A}_p$ conform to

$$\lambda_{p+1,j} = h\, \lambda_{p,j}, \quad h > 1 \tag{26}$$

and lead to a stable closed loop, i.e. $Re\{\lambda_p\} < 0$. These controllers thus accelerate the control system's behavior, while simultaneously causing a similar behavior, since the eigenvalue configuration remains the same.

In a second step the Lyapunov regions are constructed employing quadratic Lyapunov functions $v_p(x) = x^T R_p x$,

---

[4]A common practice, as we do in this section, is that of choosing $u_{dVSC}(t) = K_p x(t)$.

---

where the matrix $R_p$ is the solution of the Lyapunov equation $\hat{A}_p^T R_p + R_p \hat{A}_p = -Q_p$.

The matrices $Q_p$ have to be positive-definite: $Q_{p+1} = Q_p$ is frequently a reasonable choice. Thus, the Lyapunov regions will be ellipses determined by the matrices $R_p$. Since the condition $|K_p x| \leq u_{\max}$ has to be satisfied for all $x \in G_p$ and should be exploited as good as possible, the $c_p$ in (24) are chosen such that the hyperplanes $\pm K_p x = u_{\max}$ are tangent to the elliptical Lyapunov regions. In order to determine these $c_p$ we solve the optimization problem

$$\begin{cases} \max_{R_p} & x^T R_p\, x \\ \text{s.t.} & \pm K_p\, x = u_{\max} \end{cases} \tag{27}$$

whose solution yields

$$c_p = \frac{u_{\max}^2}{K_p\, R_p^{-1} K_p^T}. \tag{28}$$

The largest Lyapunov region $G_1$ has to be determined such that $X_0 \subseteq G_1$, i.e. the first region includes all possible initial states.

Finally, in a third step we verify that all regions $G_p$'s are nested: if all points of interest satisfy

$$\frac{x^T R_p\, x}{c_p} < \frac{x^T R_{p+1}\, x}{c_{p+1}} < 1 \tag{29}$$

then $G_{p+1} \subset G_p$ is ensured. To check whether (29) is true or not it is sufficient to make sure that the matrices

$$\frac{R_{p+1}}{c_{p+1}} - \frac{R_p}{c_p} \tag{30}$$

are positive definite for $p = 1, \ldots, m - 1$.

## V. EXPLICIT MODEL PREDICTIVE CONTROL

*Model Predictive Control* (MPC) [4], also referred as *moving horizon control* or *receding horizon control*, is an advanced control method that has become an attractive feedback strategy, especially for linear and time-invariant systems of the form (10) under the constraint (12), that are those of interest here.

The basic idea of MPC is the following: at every time step, the control action is chosen solving an optimal control problem, minimizing a performance criterion over a future horizon. Only the first control command will be applied and after one time step other measurements will be got and the optimization problem is repeated. This is an on-line procedure and in many cases it is difficult (or even impossible) to implement because the on-line solution of a linear or quadratic program, depending on the performance index, is required. Various MPC algorithms use different cost functions to obtain the control action. In this paper we consider the following standard form:

$$J(x(k), u(k), N) = \sum_{j=0}^{N} x(k+j)^T Q x(k+j) + u(k+j)^T R u(k+j) \tag{31}$$

where $Q$ and $R$ are positive definite matrices.

The main limitation of the implicit MPC is that the computations are executed on-line, so that it is only applicable to relatively slow and/or small problems.

The eMPC approach is based on multiparametric programming. It moves all the burdensome computations off-line and partitions the state space into polytopic regions, so that during the on-line phase of the control procedure according to the current state the actual subcontroller can be found out of a table. The on-line phase of the eMPC is similar to that one of the other approaches presented above (OGS and dVSC).

In this paper, in order to avoid repeating results already published in other papers [3], [5] we do not provide details on how the polytopic regions are computed. Moreover, the eMPC controller can be computed using the Multi-Parametric Toolbox called MPT [12], a free and user-friendly MATLAB toolbox for design, analysis and deployment of optimal controllers for constrained linear and hybrid systems.

As already pointed out by the authors in [3], [5], the main drawback of the eMPC is that it may easily lead to controllers with prohibitive complexity, both in runtime and solution. In particular, there are three aspects which are important in this respect: performance, closed-loop stability and constraint satisfaction. The MPT toolbox provides several possibilities to compute the controller and the partition of the state space, which are specified below and that we have investigated.

— *Finite Time Optimal Control (FTOC)*. This method yields the finite time optimal controller, i.e. the performance will be $N$-step optimal but may not be infinite horizon optimal. The complexity of the controller depends strongly on the prediction horizon $N$, the larger $N$ the more complex the controller is. Furthermore, within this method, the MPT toolbox provides three different modes.

• `probstruct:Tconstraint=0`: The controller will be defined over a superset of the maximum controllable set (i.e. all states, which are controllable to the origin), but no guarantees on stability or closed-loop constraint satisfaction can be given. As the prediction horizon $N$ is increased the feasible set of states will converge to the maximum controllable set from "the outside-in", i.e., the controlled set will shrink as N increases.
Even though closed loop stability and constraint satisfaction are not guaranteed, MPT provides a function to extract the set of states which satisfy the constraints for all time and another function to analyze these states for stability.

• `probstruct:Tconstraint=1`: The resulting controller will guarantee stability and constraint satisfaction for all time, but will only cover a subset of the maximum controllable set of states. By increasing the prediction horizon, the controllable set of states will converge to the maximum controllable set from "the inside-out", i.e. the controlled set will grow larger as $N$ increases.

— *Infinite Time Optimal Control (ITOC)*. This method yields the infinite time optimal controller, i.e. the best possible performance for the control problem. Asymptotic stability and constraint satisfaction are guaranteed and the maximum controllable set will be covered by the resulting
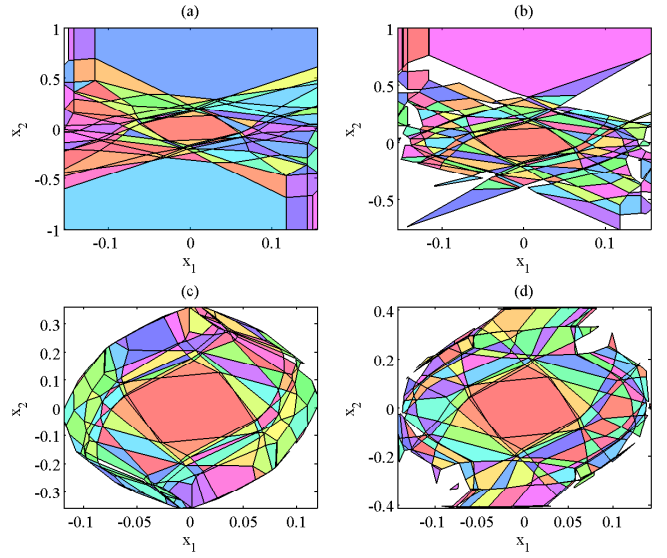


Fig. 2. The resulting partitions in the fourth-order case (cut through $x_3 = x_4 = 0$). (a) FTOC, `probstruct:Tconstraint=0`, $N = 10$, 557 regions; (b) FTOC, `probstruct:Tconstraint=0`, $N = 15$, 1038 regions; (c) FTOC , `probstruct:Tconstraint=1`, $N = 10$, 2195 regions; (c) FTOC , `probstruct:Tconstraint=1`, $N = 15$, 3852 regions.

controller. However, the controller's complexity may be prohibitive and the computation may take a very long time.

Two other options are possible when designing the eMPC controller using the toolbox MPT, namely *Minimum Time Control* and *Low Complexity Control*. However, we do not discuss these cases here because we have not been able to apply them to our application: in both cases the computation did not finish in adequate times.

## VI. A COMPARISON AMONG THE DIFFERENT APPROACHES

In this section we compare the three control design methods above applying them to the suspension system illustrated in Section II.

Following [8], we take: $M_w = 28.58$ Kg, $M_s$=288.90 Kg, $\lambda_t = 155900$ N/m, $\lambda_s = 14345$ N/m. We assume the sampling time equal to $T = 0.01$ s, to which it corresponds the sampling frequency $\omega_s = 2\pi/T \simeq 6 \cdot 10^2$ rad/s[5].

We take $u_{\max} = 3000$ N that is slightly less than the total weight resting on one wheel. A control force of higher magnitude may cause loss of contact between wheel and road. Furthermore, this constraint also limits the acceleration of the sprung mass and this is a necessary condition for the comfort of passengers.

[5]This is essentially due to the following reasons. Firstly, the bandwidth of the passive suspension system described by (3) is $\omega_b < 2 \cdot 10^2$ rad/s. A sampling frequency of $\omega_s \simeq 6 \cdot 10^2$ rad/s is in good agreement with Shannon's theorem [13] that requires $\omega_s > 2\omega_b$. Moreover, this choice of sampling interval is consistent ensures that the system will maintain the properties of controllability and observability. Finally, to change $f$ the controller must change the opening of the damper valve. Present technologies impose a limit of about $10^2$ Hz on the updating frequency of the damper coefficient.

Finally we choose $f(k) \in [800, 3000]$ Ns/m.

For the OGS approach we consider two different cases.

— *OGS (Case A)* When dealing with the fourth order model we assume $Q = [11 - 1\ 0\ 0; -1\ 1\ 0\ 0; 0\ 0\ 0\ 0; 0\ 0\ 0\ 0]$ and $R = 0.8 \cdot 10^{-9}$, that lead to a good performance in terms of road holding and passenger's comfort. Finally, as in [8] we choose the parameters $\rho_i$'s as follows: $\rho_1 = 0.01$, $\rho_2 = 0.1$, $\rho_3 = 0.5$, $\rho_4 = 1$, $\rho_5 = 4$, $\rho_6 = 20$, $\rho_7 = 50$, $\rho_8 = 100$, $\rho_9 = 1000$, $\rho_{10} = 10^5$. When dealing with the second order model we assume $Q = [1\ 0; 0\ 0]$, $R = 0.8 \cdot 10^{-9}$, and $\rho_1 = 0.5$, $\rho_2 = 1$, $\rho_3 = 4$, $\rho_4 = 20$, $\rho_5 = 50$.

— In the case of the fourth-order model with dVSC controller we assume the set of eigenvalues reported in Fig. 4.b. The first set of eigenvalues in (26) was chosen according to the closed loop eigenvalues of the OGS for the fourth largest region, while the remaining four are chosen assuming $h = 1.5$ in (26). In the case of the second-order model with dVSC controller we assume $\lambda_{1,2} = -7.8224 \pm 7.8224j$, $h = 1.5$ and $m = 5$.

— *OGS (Case B)* In order to obtain a more immediate and meaningful comparison among the OGS and the dVSC approach, we determined the feedback gain matrices for the OGS controller such that the closed loop eigenvalues in the OGS case are the discrete-time counterpart of the dVSC closed loop eigenvalues. As an example, in the case of the fourth order model, the closed loop eigenvalues are those shown in Fig. 4.a. Note that the closed loop matrices obtained in this manner do not guarantee that the Yoshida regions are nested.

— For the eMPC we considered the same weighting matrix on the states ($Q$) as in the OGS (Case A). The weight on the input is taken equal to the weight on the input for the OGS (Case A) divided by $\rho_{max}$, i.e., $R_{eMPC} = R/\rho_{max}$. This guarantees for both approaches the same level of optimality.

### A. Some remarks on eMPC

In this section we highlight some problems we encountered when applying the eMPC to the fourth-order model. Let us first observe that in order to reduce the run times we determined the partition of the state space for the fourth-order suspension model considering: $X = \{x \in \mathbb{R}^4 \mid |x_i| \leq 1, i = 1, \ldots, 4\}$.

In order to clarify which kind of problems we get into, we reported in Fig. 2 some of the resulting partitions, where a cut at $x_3 = x_4 = 0$ is done. The results relative to the FTOC case with `probStruct. Tconstraint=0` are shown in Fig. 2.a and b: increasing the prediction horizon $N$ from 10 to 15 the controlled set converges towards the maximum controllable set from the outside inwards. As expected the partition in figure (a) cover a larger set than the partition in figure (b).

The partitions for the FTOC employing `probStruct.Tconstraint=1` are illustrated in Fig. 2.c and d for $N = 10$ and $N = 15$, respectively. As mentioned above, by increasing the prediction horizon $N$ the controllable set should converge to the maximum
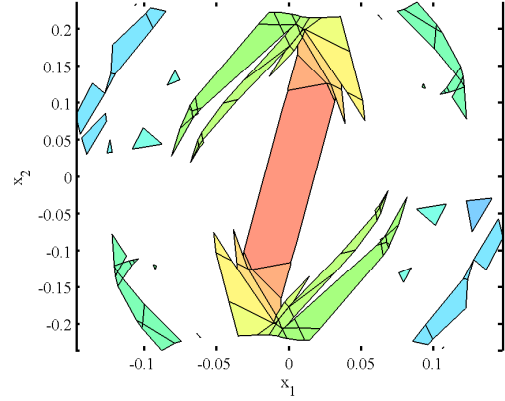


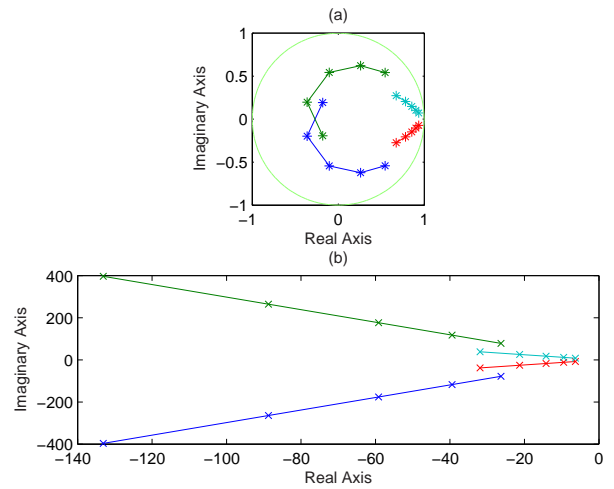Fig. 3. Projection of the partition into the $x_1$-$x_2$-plane for the fourth-order suspension system for the ITOC



Fig. 4. Sets of designated eigenvalues for the fourth-order suspension system (a) in the z-plane and (b) in the s-plane. $h = 1.5$

controllable set from the inside outwards. Clearly, this is not occurring in this case because parts of the state space that have been covered by the partition with $N = 10$ are not covered by the partition obtained with $N = 15$. Thus, we conclude that some numerical error should have occurred: it is obviously not possible that a state is controllable under a given prediction horizon, but does not maintain this property after increasing the latter.

In the case of the ITOC the unfeasability of the result is even more evident as illustrated in Fig. 3. Only very few parts of the state space that were identified to be controllable (see Fig. 2.c) are covered by the ITOC partition.

### B. A comparison among partitions

Fig. 5 shows the different state space partitions in the case of the second-order suspension model: the Yoshida regions for the OGS (Case A) and (Case B) are depicted in Fig. 5.a and b, respectively; figures c and d illustrate the regions resulting from dVSC and eMPC, respectively.

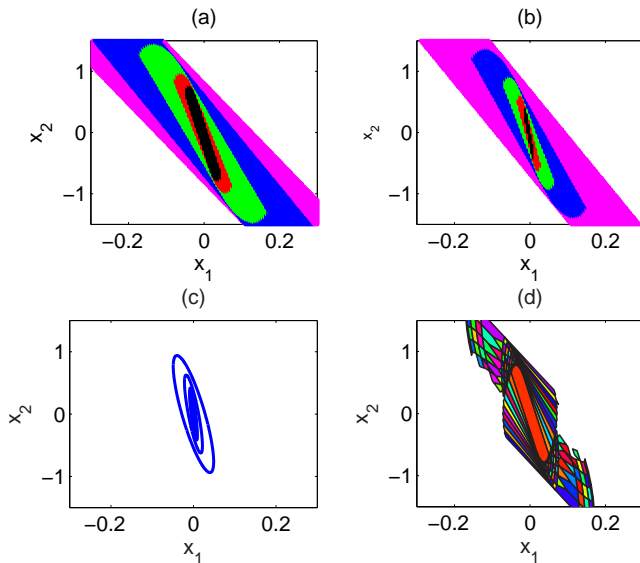Note that in order to limit the run times of the computation

Fig. 5. Partition of the state space for the second-order model: (a) OGS (Case A); (b) OGS (Case B); (c) dVSC; (d) eMPC.



Fig. 6. A cut at $x_3 = x_4 = 0$ of the regions obtained for the fourth-order model: (a) OGS (Case A) (b) eMPC.

of the polytopic regions employing eMPC we considered the following bounded polyhedron for the second-order suspension model: $X = \{x \in \mathbb{R}^2 \mid |x_i| \leq 1, \ i = 1, 2\}$. Furthermore, we considered the FTOC with a prediction horizon $N = 10$ and we set probStruct.Tconstraint=1 to obtain a controller that guarantees closed loop stability and constraint satisfaction for all times.

By looking at Fig. 5 we realized that: the OGS regions are those who cover the largest portion of the state space, while the dVSC's cover the smallest portion of the state space. Then, also in Case B the OGS regions are nested, thus we can use them to design a controller. Finally, we observe that the eMPC regions are constrained in the $x_2$-direction by the assumptions we made in order to reduce the run time (i.e., $x \in X$), but also in the $x_1$-direction they are smaller than the OGS regions (Cases A and B).

Fig. 6 depicts a cut through $x_3 = x_4 = 0$ of the partitions obtained with the fourth-order model resulting from the OGS (Case A) and the eMPC. Here the difference on the size of two state space partitions is even more evident.

We have not reported here the regions obtained when implementing the OGS (Case B) and the dVSC with the the fourth-order model, because in the OGS case the regions were not nested, and in the dVSC case they cover a too small portion of the state space with respect to the nominal operating conditions. Thus they are both useless for the considered application.

Some important remarks should be done to interpret the above results. In the dVSC case the size of the regions depends on $R_p$ and therefore on the choice of $Q_p$ in the Lyapunov equation. Because $c_p$, that determines the Lyapunov regions, is a function of $R_p^{-1}$, the regions seem to be nearly independent on the choice of $Q_p$. As a consequence, we have not been able to enlarge the Lyapunov regions significantly
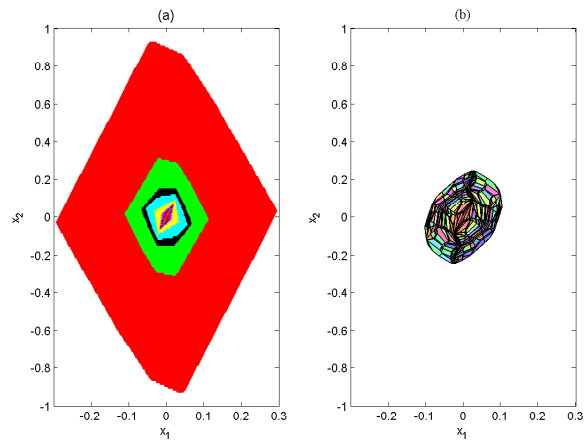
acting on $Q_p$.

Note that this problem cannot be overcome using soft VSC rather than dVSC [2]. This is the reason why we do not go on details of soft VSC in this paper.

In the eMPC case the size of the covered state space is related to different issues, namely, the constraints on the states ($x \in X$) we introduce to implement the procedure, the options we choose (see the discussion above relative to the setting of parameters in the MPT toolbox), and, in the case of FTOC, the prediction horizon $N$.

As a result, we draw the following conclusions. (1) The dVSC regions cover a very small subset of the state space of interest, but the computational effort is very low. (2) The OGS (Case A) seems to lead to the best results both in terms of computational effort and in terms of dimension of the state space partition. (3) The eMPC provides intermediate results in terms of size of the state space partition, and is the hardest in terms of computational complexity and implementation.

### C. The control performance: second-order model

In the case of active suspensions we only present the results of numerical simulations carried out on the second order model, because in such a case all the considered techniques provide state space partitions that are large enough to deal with realistic cases.

We computed the system's evolution for the initial state $x_0 = [0.01 \ 0.1]^T$. The simulation results are summarized in Fig. 7. We can observe that the OGS (Case A) and the eMPC provide satisfactory results, and the system evolution is practically the same in the two cases. On the contrary, the results obtained with the dVSC controller are not so satisfactory: this is due to the fact that it does not yield a good exploitation of the maximal allowed control input. The OGS controller (Case B) provides the best performance in terms of sprung mass position, but its behaviour is less satisfactory in terms of sprung mass velocity and acceleration. Finally, in the right bottom graph of Fig. 7 we have pointed out the variation of the index denoting the current region of the state
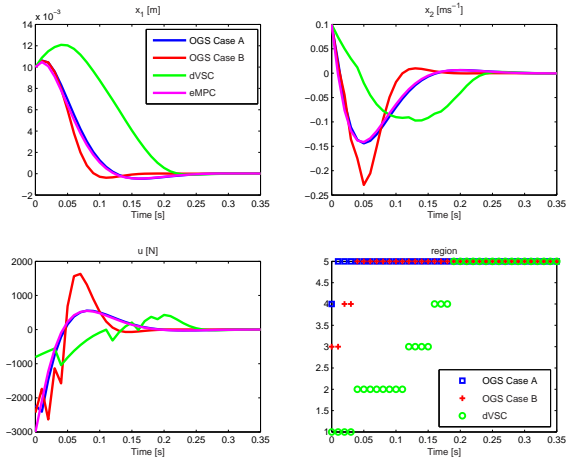
Fig. 7. Active suspension and initial state $x_0 = [0.01\ 0.1]^T$.

space in the OGS cases (A and B) and in the dVSC case. Here 1 denotes the largest region and 5 the smallest one.

### D. The control performance: fourth-order model

In this section we compare the simulation results for the fourth-order suspension model.

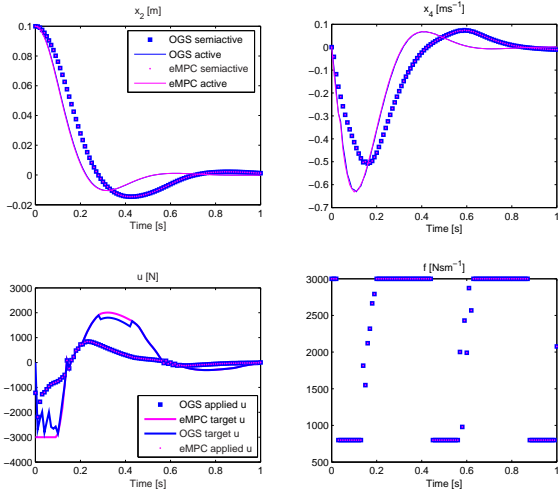Assume that the initial state is $x_0 = [0.015\ 0.1\ 0\ 0]^T$.



Fig. 8. Semiactive suspension with $x_0 = [0.015\ 0.1\ 0\ 0]^T$.

Fig. 8 shows the evolution of the semiactive suspension system compared to that of the active suspension. Again the OGS and the eMPC performances are very similar as the states at each time instant only differ in the order of magnitude of $|x_{i,\text{OGS}} - x_{i,\text{eMPC}}| \approx 10^{-10}$. In the bottom left of Fig. 8 we have reported the evolution of the target control laws computed with the OGS and the eMPC, and the control laws that are "really" applied to the system by the semiactive suspension when appropriately adjusting the damping coefficient $f$ (whose variation is shown in the bottom right of Fig. 8).

## VII. CONCLUSIONS

In this paper we deal with the problem of designing a semiactive suspension system for car vehicles. To this aim we considered three different techniques, namely *optimal gain switching*, discontinuous VSC and *explicit MPC*. All these approaches are based on the computation of an off-line partition of the state space. To each convex region a linear or an affine control law is associated, and the on-line phase of the approaches simply consists in selecting the current region. A detailed comparison among these techniques is provided, both in terms of magnitude of the resulting state space partitions, and in terms of the system behaviour. As a result, in this application the OGS controller proved to be the most effective of the three approaches in terms of performance, applicability and computational complexity.

## ACKNOWLEDGMENTS

## REFERENCES

[1] Adamy, J.: Strukturvariable Regelungen mittels impliziter Ljapunov-Funktionen. Ph.D dissertation (1991), University of Dortmund.
[2] Adamy, J. and Flemming, A.: Soft variable-structure controls: a survey, *Automatica* 40 (2004), pp. 1821–1844.
[3] Bemporad, A., Morari, M., Dua, V. and Pistikopoulos, E.N.: The explicit linear quadratic regulator for constrained systems, *Automatica* 38 (2002), pp. 3-20.
[4] Bemporad, A., Torrisi, F.D. and Morari, M., Performance Analysis of Piecewise Linear Systems and Model Predictive Control Systems, *Proc. of the 39th IEEE Conference on Decision and Control*, Sydney, Australia, 2000, pp. 4957-4962.
[5] Borrelli, F.: Discrete time constrained optimal Control, Ph.D dissertation (2002), ETH Zurich.
[6] Cheok, K.C., Loh, N.K., McGree, H.D. and Petit, T.F.: Optimal model following suspension with microcomputerized damping, *IEEE Trans. on Industrial Electronics*, Vol. 32, No. 4, November 1985.
[7] Giorgetti, N., Bemporad, A., Tseng, H. E. and Hrovat, D.: Hybrid model predictive control application towards optimal semi-active suspension, *Proc. IEEE Int. Symp. on Industrial Electronics*, Dubrovnik, Croatia (2005).
[8] Giua, A., Seatzu, C. and Usai, G.: Semiactive Suspension Design with an Optimal Gain Switching Target, *Vehicle Systems Dynamics*, 31(1999), pp.213–232.
[9] Hac, A.: Suspension optimisation of a 2-DOF vehicle model using a stochastic optimal control technique, *Journal of Sound and Vibration*, Vol. 100, No. 3, pp. 343–357, 1985.
[10] Kiendl, H., and Schneider, G.: Synthese nichtlinearer Regler fuer die Regekstrecke const/s$^2$ aufgrund ineinandergeschalchtelter abgeschlossener Gebiete beschraenkter Stellgroesse, *Regelungstechnik und Prozess-Datenverarbeitung*, 20(7) (1972).
[11] Krasnicki, E. J.: Comparison of analytical and experimental results for a semi-active vibration isolator, *The Shock and Vibration Bulletin*, pt. 4, pp. 69–76, September 1980.
[12] Kvasnica, M., Grieder, P. and Baotic, M.: Multi-Parametric Toolbox (MPT), http://control.ee.ethz.ch/ mpt/, (2004).
[13] Ogata, K.: Discrete-time control systems, Prentice Hall International Editions, 1972.
[14] Thompson, A.G.: An active suspension with optimal linear state feedback, *Vehicle System Dynamics*, Vol. 5, pp. 187–203, 1976.
[15] Wonham, W.M. and Johnson C.D.: Optimal bang-bang control with quadratic performance index, *Trans. ASME Journal of Basic Engineering*, Vol. 86, pp. 107–115, March 1964.
[16] Yoshida, K., Nishimura, Y. and Yonezawa, Y.: Variable gain feedback control for linear sampled-data systems with bounded control, *Control Theory and Advanced Technology*, 2(2) (1986).